Bulletin of Pure and Applied Sciences.
Vol.41 D (Physics), No.2,
July-December 2022 P. 116-128

Print version ISSN 0970 6569
Online version ISSN 2320 3218

Original Research Article

Available online at www.bpasjournals.com

Double-Folding Model Potentials with M3Y and São Paulo Interactions: Constructing Realistic Nucleus–Nucleus Potentials and Comparing Barrier Predictions

Dr. Rahul Kumar[1]

Author's Affiliations:

Dr. Rahul Kumar [1]Assistant Professor (GT), Department of Physics, H.R. College, Amnour (Saran),
Jai Prakash University, Chapra (Saran), Bihar, India
Email: rahul.nishu@yahoo.com

***Corresponding author:** **Dr. Rahul Kumar**
Assistant Professor (GT), Department of Physics, H.R. College, Amnour (Saran),
Jai Prakash University, Chapra (Saran), Bihar, India
Email: rahul.nishu@yahoo.com

ABSTRACT

The nucleus–nucleus interaction potential is the central quantity that governs elastic scattering, sub-barrier fusion, and the formation of compound and super-heavy systems. Among microscopic prescriptions, the double-folding model occupies a privileged position because it constructs the real part of the heavy-ion potential directly from the matter densities of the colliding nuclei and an effective nucleon–nucleon interaction, thereby minimising the number of adjustable parameters. This article develops the double-folding formalism in a self-contained manner and applies it with two of the most widely used effective interactions: the density-independent M3Y (Michigan three-range Yukawa) force in its Reid parametrisation, supplemented by a knock-on exchange term, and the São Paulo interaction, in which the folded potential is multiplied by a velocity-dependent factor that encodes the Pauli nonlocality. The folding integral is evaluated in momentum space, the resulting nuclear potential is combined with the Coulomb and centrifugal terms, and the fusion barrier height, radius, and curvature are extracted. For a representative set of eight systems spanning ^12C+^12C to ^48Ca+^208Pb, both interactions reproduce empirical barrier heights to within a few percent without any renormalisation, the São Paulo prescription tending to predict marginally higher and more compact barriers. Fusion excitation functions are further computed in the Wong approximation, and the sensitivity of the barrier to the surface diffuseness and to the energy dependence of the interaction is analysed. The results demonstrate that parameter-free folded potentials provide a reliable and physically transparent foundation for heavy-ion reaction studies....

KEYWORDS Double-folding model, M3Y interaction, São Paulo potential, Coulomb barrier, Heavy-ion fusion, Pauli nonlocality...

INTRODUCTION

The interaction potential between two atomic nuclei is the single most important ingredient in the,

quantitative description of low-energy heavy-ion reactions [1, 2]. Whether one seeks to fit an elastic-scattering angular distribution, to predict a sub-barrier fusion excitation function, or to estimate the survival probability of a freshly formed super-heavy nucleus, the calculation ultimately rests on a model of how the projectile and target attract and repel one another as a function of their separation. For decades the practical workhorse has been the phenomenological Woods–Saxon form, whose depth radius, and diffuseness are adjusted to reproduce data [3]. While flexible, such a purely empirical approach offers little predictive power for systems where,..

measurements are scarce, and it has become increasingly clear that a single Woods–Saxon shape cannot simultaneously describe elastic scattering and fusion [4].

A more fundamental route is provided by the folding model, in which the real nuclear potential is generated microscopically [5, 6]. In the double-folding model the potential is obtained by integrating an effective nucleon–nucleon interaction over the matter distributions of both nuclei, so that the only inputs are the nuclear densities, which are well constrained by electron scattering and by mean-field theory [7, 8], and the effective interaction, which is calibrated once and for all to nucleon–nucleon scattering and nuclear-matter properties. The resulting potential carries genuine predictive content: the same interaction that describes one system is applied unchanged to all others. This economy of parameters is precisely what makes the folding model attractive as a benchmark against which phenomenological potentials and dynamical models can be assessed.

Two families of effective interactions dominate contemporary applications. The first is the M3Y interaction [9], constructed by the Michigan group from a sum of three Yukawa terms whose ranges are fixed by the one-pion-exchange tail and by the exchange of heavier mesons, with strengths fitted to G-matrix elements of a realistic nucleon–nucleon force. The M3Y interaction, augmented by a knock-on exchange contribution, has provided successful descriptions of elastic and inelastic scattering across a wide energy range [10, 11]. The second is the São Paulo interaction [12, 13], which retains the folding philosophy but multiplies the folded potential by a velocity-dependent factor that accounts for the nonlocality arising from the Pauli exclusion principle. The São Paulo potential has been applied, essentially without free parameters, to hundreds of systems and energies [14, 15].

The purpose of this article is to present a unified and reproducible account of how realistic nucleus–nucleus potentials are constructed from these two interactions, and to compare in detail the Coulomb-barrier predictions they yield. Section 2 sets out the methods: the folding formalism, the two effective interactions, the nuclear densities, the momentum-space evaluation of the folding integral, and the determination of the barrier and the fusion cross section. Section 3 presents the resulting potentials, barrier systematics, energy dependence, and fusion excitation functions for a set of benchmark systems. Section 4 discusses the physical content of the comparison, its limitations, and directions for further work, and Section 5 summarises the conclusions.

Notation: Throughout this article, vectors are written in bold (for example **R** for the relative separation and **r** for an intrinsic coordinate), and the corresponding light-italic symbol denotes the magnitude. Energies are quoted in MeV, lengths in fm, and the elementary product $e^2 = 1.44$ MeV·fm is used for the Coulomb interaction. Bold font applied to key terms in the running text marks their first introduction and carries no mathematical meaning.

2. Methods

2.1 The Double-Folding Formalism

The real part of the nucleus–nucleus interaction is obtained in the double-folding model by averaging an effective nucleon–nucleon interaction v_{NN} over the ground-state matter distributions ρ_1 and ρ_2 of the two nuclei [5]. Writing **R** for the vector joining the two centres, the folded potential reads

$$V_{DF}(\mathbf{R}) = \iint \rho_1(\mathbf{r}_1)\,\rho_2(\mathbf{r}_2)\,v_{NN}(s)\,d^3r_1\,d^3r_2, \qquad \mathbf{s} = \mathbf{R} + \mathbf{r}_2 - \mathbf{r}_1. \tag{1}$$

Here s is the separation between a nucleon in the projectile and a nucleon in the target, and the densities are normalised to the respective mass numbers,

$$\int \rho_i(\mathbf{r})\,d^3r = A_i, \qquad i = 1{,}2. \tag{2}$$

The total interaction in a given partial wave l combines the nuclear potential with the Coulomb and centrifugal terms,

$$V(R) = V_N(R) + V_C(R) + \frac{\hbar^2\, l(l+1)}{2\mu R^2}, \qquad (3)$$

where $\mu = m_N A_1 A_2/(A_1 + A_2)$ is the reduced mass and m_N the nucleon mass. The nuclear term V_N is identified with the folded potential of Equation (1), to which an exchange contribution is added as described below. The competition between the long-range Coulomb repulsion and the short-range nuclear attraction produces the **Coulomb barrier**, whose height and position control fusion and elastic scattering near the barrier. The complete construction, from the input matter densities and effective interaction through the folding integral to the total potential and the barrier and fusion observables, is summarised schematically in Figure 1.

2.2 The M3Y Effective Interaction

The M3Y interaction represents the effective force as a sum of Yukawa functions whose ranges reproduce the one-pion-exchange tail and simulate the exchange of heavier mesons [9]. The direct part is written

$$v_D(s) = \sum_i V_i\, \frac{e^{-\mu_i s}}{\mu_i s}, \qquad (4)$$

and in the widely used Reid parametrisation [16] the two effective ranges and strengths are

$$v_D^{\mathrm{Reid}}(s) = 7999\, \frac{e^{-4s}}{4s} - 2134\, \frac{e^{-2.5s}}{2.5s} \ \text{MeV}, \qquad (5)$$

with s in fm. The longer-range, attractive term ($\mu = 2.5$ fm^{-1}) dominates at the nuclear surface, while the shorter-range, repulsive term ($\mu = 4$ fm^{-1}) provides the inner repulsion. An alternative calibration based on the Paris potential, denoted M3Y-Paris, employs the stronger strengths 11061.6 and -2537.5 MeV with the same ranges. The radial dependence of the direct M3Y interaction in both the Reid and Paris parametrisations is shown in Figure 2.

Antisymmetrisation of the two-nucleon wave function generates a knock-on **exchange** term. Because the exchanged-nucleon overlap is of very short range, it is conveniently represented by an energy-dependent zero-range pseudopotential,

$$v_{EX}(s, E) = J_{00}(E)\, \delta(\mathbf{s}), \qquad J_{00}(E) = -276\left(1 - 0.005\, \frac{E}{A_p}\right) \text{MeV}\cdot\text{fm}^3, \qquad (6)$$

where E is the bombarding energy and A_p the projectile mass number. The energy-slope coefficient of 0.005 MeV^{-1} is the standard value for the M3Y-Reid exchange pseudopotential [5]; the Paris calibration adopts a slightly smaller slope, but the difference is immaterial at the near-barrier energies considered here. Folding the zero-range exchange reduces to the density overlap,

$$V_{EX}(R) = J_{00}(E) \int \rho_1(\mathbf{r})\, \rho_2(\mathbf{R} - \mathbf{r})\, d^3 r, \qquad (7)$$

so that the complete M3Y nuclear potential is the sum

$$V_N^{\mathrm{M3Y}}(R) = V_D(R) + V_{EX}(R). \qquad (8)$$

The bare M3Y interaction does not reproduce the saturation of nuclear matter; this deficiency is remedied in density-dependent variants (DDM3Y, BDM3Y) [17, 18] by multiplying v_{NN} with a factor $g(\rho) = C(1 - \beta\, \rho^n)$ [11]. The present article retains the original density-independent form, which is adequate at and below the barrier, and notes the density-dependent extension where relevant.

2.3 The São Paulo Interaction and Pauli Nonlocality

The **São Paulo potential** (SPP) begins from the same folding prescription but recognises that the bare folded potential is a local approximation to an intrinsically nonlocal interaction [12, 13]. The nonlocality,

which originates in the exchange of identical nucleons forbidden by the Pauli principle, is mapped onto a local but velocity-dependent potential,

$$V_{SP}(R,E) = V_F(R)\, e^{-4v^2/c^2}, \qquad (9)$$

where c is the speed of light and v is the local relative velocity between the nuclei, determined self-consistently from energy conservation,

$$v^2(R,E) = \frac{2}{\mu}[E - V_C(R) - V_N(R,E)]. \qquad (10)$$

The folded form factor V_F in the original São Paulo prescription is evaluated with a zero-range effective interaction whose strength reproduces the volume integral of the M3Y force,

$$V_F(R) = v_0 \int \rho_1(\mathbf{r})\, \rho_2(\mathbf{R}-\mathbf{r})\, d^3r, \qquad v_0 = -456 \text{ MeV}\cdot\text{fm}^3. \qquad (11)$$

The exponential damping in Equation (9) reduces the depth of the potential as the relative velocity increases, which translates into the experimentally observed energy dependence of the heavy-ion optical potential. Because the velocity itself depends on V_N, Equations (9) and (10) must be solved iteratively at each radius and energy.

2.4 Nuclear Matter Densities

Both interactions are folded over realistic matter distributions, for which the **two-parameter Fermi** (2pF) form is used,

$$\rho(r) = \frac{\rho_0}{1 + \exp[(r - R_0)/a]}, \qquad (12)$$

with the central density ρ_0 fixed by the normalisation of Equation (2). The radius and diffuseness follow the São Paulo systematics extracted from a global analysis of charge and matter distributions [14],

$$R_0 = 1.31\, A^{1/3} - 0.84 \text{ fm}, \qquad a = 0.56 \text{ fm}. \qquad (13)$$

The associated root-mean-square radius,

$$\langle r^2 \rangle^{1/2} = \left[\frac{4\pi}{A}\int_0^\infty r^4\, \rho(r)\, dr\right]^{1/2}, \qquad (14)$$

reproduces the empirical trend $\langle r^2 \rangle^{1/2} \approx 0.95\, A^{1/3}$ fm. Table 1 lists the resulting parameters for the nuclei considered in this work.

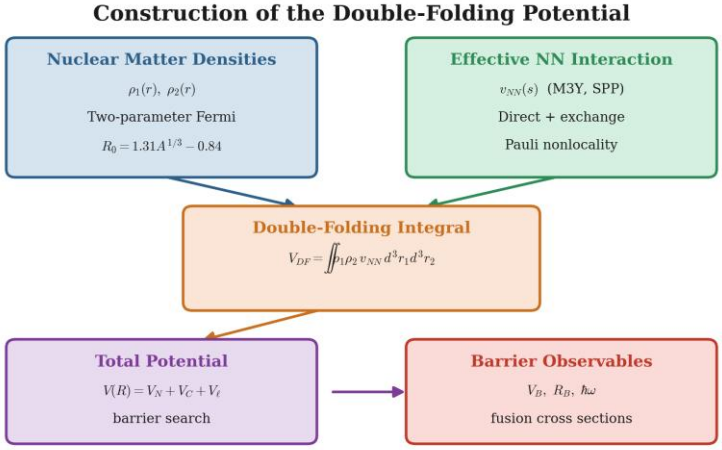

Figure 1. ***Schematic of the double-folding construction. The nuclear matter densities of the two***

nuclei and the effective nucleon–nucleon interaction (M3Y or São Paulo) are combined in the double-folding integral to produce the nuclear potential; addition of the Coulomb and centrifugal terms yields the total potential, from which the barrier height, radius, curvature, and fusion cross sections are extracted.

2.5 Momentum-Space Evaluation of the Folding Integral

The six-dimensional integral in Equation (1) is most efficiently evaluated in momentum space, where the convolution theorem reduces it to a one-dimensional radial integral [5]. For spherical densities and interactions one obtains

$$V_{DF}(R) = \frac{1}{2\pi^2 R}\int_0^\infty q\,\sin(qR)\,\tilde{\rho}_1(q)\,\tilde{\rho}_2(q)\,\tilde{v}(q)\,dq, \qquad (15)$$

where the Fourier transform of a spherical density is

$$\tilde{\rho}(q) = \frac{4\pi}{q}\int_0^\infty r\,\sin(qr)\,\rho(r)\,dr, \qquad (16)$$

and the transform of a single Yukawa term is analytic,

$$\tilde{v}(q) = \frac{4\pi V}{\mu(\mu^2+q^2)}. \qquad (17)$$

The zero-range exchange and São Paulo form factors involve only the density overlap, whose transform is $\tilde{\rho}_1(q)\,\tilde{\rho}_2(q)$ with $\tilde{v}(q)$ replaced by the constant J_{00} or v_0, respectively. All integrals are performed on a momentum grid extending to $q = 8$ fm^{-1}, which is amply converged for the densities of Equation (12).

2.6 Construction of the Total Potential and Barrier Search

The Coulomb interaction is taken as that of a uniformly charged sphere of radius $R_C = 1.2\left(A_1^{1/3} + A_2^{1/3}\right)$ fm,

$$V_C(R) = \begin{cases} \dfrac{Z_1 Z_2 e^2}{2R_C}\left(3 - \dfrac{R^2}{R_C^2}\right), & R \le R_C, \\ \dfrac{Z_1 Z_2 e^2}{R}, & RR_C, \end{cases} \qquad (18)$$

which coincides with the point-charge form in the barrier region, where the charge distributions barely overlap. The s-wave barrier is located by the stationarity conditions

$$\left.\frac{dV}{dR}\right|_{R_B} = 0, \qquad \left.\frac{d^2V}{dR^2}\right|_{R_B} 0, \qquad (19)$$

and the local curvature defines the barrier frequency

$$\hbar\omega = \hbar\sqrt{\frac{1}{\mu}\left|\frac{d^2V}{dR^2}\right|_{R_B}}, \qquad (20)$$

which governs the rate of barrier penetration. The barrier height V_B, radius R_B, and curvature $\hbar\omega$ constitute the three observables that fully characterise the one-dimensional barrier.

2.7 Barrier Penetration and Fusion Cross Sections

Treating the barrier as a parabola, the transmission coefficient for partial wave l is given by the Hill–Wheeler expression [19],

$$T_l(E) = \left[1 + \exp\left(\frac{2\pi(V_B^l - E)}{\hbar\omega}\right)\right]^{-1}, \qquad (21)$$

and the fusion cross section follows from the partial-wave sum $\sigma_{fus} = (\pi/k^2)\sum_l (2l+1)\ T_l$. Performing the sum in the continuous-l approximation yields the compact Wong formula [20],

$$\sigma_{fus}(E) = \frac{\hbar\omega\, R_B^2}{2E} \ln\left[1 + \exp\left(\frac{2\pi(E - V_B)}{\hbar\omega}\right)\right], \qquad (22)$$

which provides a transparent link between the static barrier parameters and the measured excitation function. As a global characteristic of the folded potential the volume integral per interacting nucleon pair is also evaluated,

$$J_V = -\frac{1}{A_1 A_2} \int V_N(R)\, d^3R, \qquad (23)$$

a quantity that is nearly system-independent for the bare M3Y force and serves as a useful consistency check.

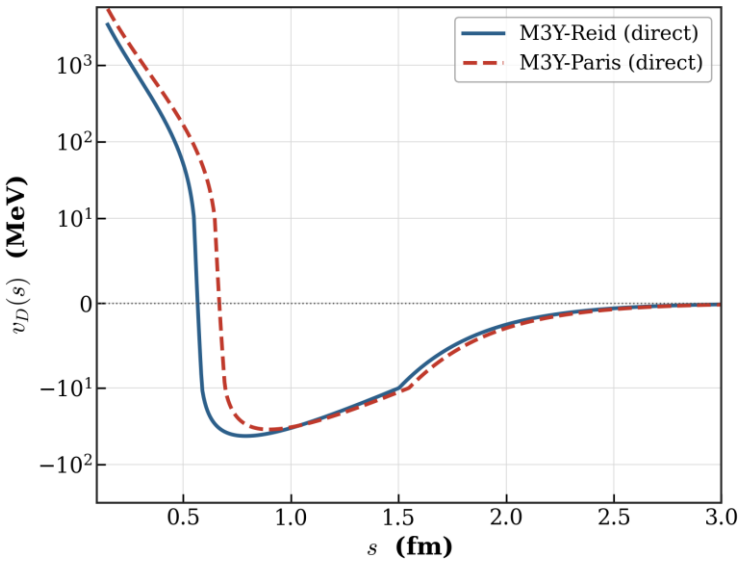

Figure 2. ***Radial dependence of the direct M3Y effective interaction in the Reid (solid) and Paris (dashed) parametrisations on a symmetric-logarithmic scale. The short-range repulsive ($\mu = 4$ fm^{-1}) and longer-range attractive ($\mu = 2.5$ fm^{-1}) Yukawa terms combine to produce an attractive tail beyond $s \approx 0.5$ fm, which dominates the folded surface potential.***

3. Results

3.1 Folded Potentials for ^{16}O + ^{208}Pb

The system ^{16}O+^{208}Pb is the canonical test case for heavy-ion potentials and is examined first. Figure 3 displays the nuclear potential obtained from the M3Y-Reid interaction with and without the knock-on exchange term, together with the bare São Paulo form factor and the velocity-damped São Paulo potential evaluated near the barrier. The direct M3Y term alone is too shallow; the addition of the zero-range exchange, Equation (7), deepens the potential by roughly a factor of three in the interior and brings the surface region into agreement with the São Paulo form factor. The velocity damping of Equation (9) reduces the São Paulo depth in the interior, where the local velocity is largest, while leaving the barrier-region tail essentially unchanged, since the two potentials are constrained to share the same volume integral.

Table 1 collects the density parameters underlying these calculations. The 2pF radius grows as $A^{1/3}$ while

the diffuseness is held fixed at the systematic value of 0.56 fm, and the central density decreases gently with mass number, reflecting the surface-to-volume ratio.

Table 1. ***Two-parameter Fermi matter-density parameters from the São Paulo systematics, Equation (13), with the resulting root-mean-square radius and central density.***

Nucleus	R_0 **(fm)**	a **(fm)**	$\langle r^2\rangle^{1/2}$ **(fm)**	ρ_0 **(fm^{-3})**
^{12}C	2.159	0.56	2.669	0.1673
^{16}O	2.461	0.56	2.822	0.1674
^{28}Si	3.138	0.56	3.200	0.1640
^{40}Ca	3.640	0.56	3.505	0.1602
^{48}Ca	3.921	0.56	3.682	0.1581
^{90}Zr	5.031	0.56	4.418	0.1504
^{144}Sm	6.026	0.56	5.111	0.1447
^{208}Pb	6.922	0.56	5.751	0.1407

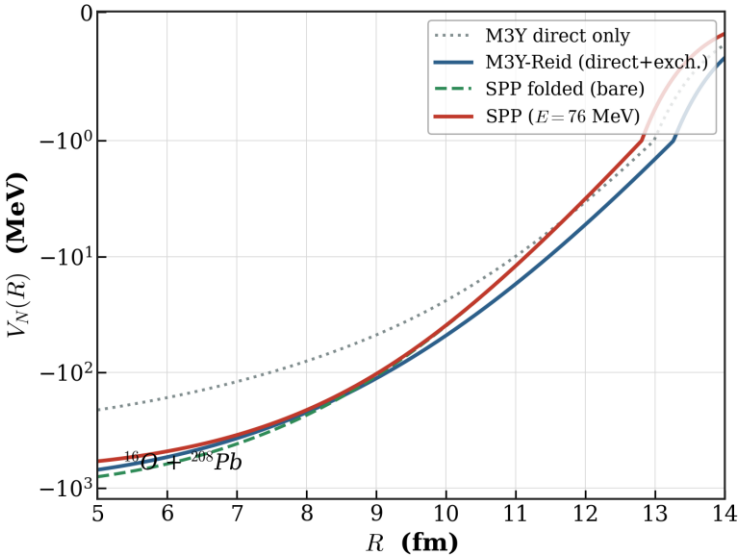

Figure 3. ***Nuclear potential for ^{16}O+^{208}Pb on a symmetric-logarithmic scale. The direct M3Y term (dotted) is substantially deepened by the knock-on exchange contribution to give the full M3Y-Reid potential (solid blue). The bare São Paulo form factor (dashed green) and the velocity-damped São Paulo potential at $E = 76$ MeV (solid red) coincide with the M3Y result in the surface region that controls the barrier.***

3.2 The Coulomb Barrier and Its Systematics

Adding the Coulomb term of Equation (18) to the nuclear potential produces the total s-wave potential shown in Figure 4. Both interactions yield a well-defined barrier near $R_B \approx 11.7$–12.0 fm. The São Paulo barrier sits about 2.5 MeV higher and 0.4 fm more compact than the M3Y-Reid barrier, a consequence

of the slightly stronger surface attraction of the velocity-damped form at the relevant separation. Beyond the barrier the two potentials are indistinguishable, as both reduce to the Coulomb tail.

Extending the analysis to the full benchmark set, Table 2 compares the predicted barrier heights and radii with empirical values compiled from fusion systematics [4, 21, 22]. Across nearly two orders of magnitude in barrier height the folded potentials track the data closely: the M3Y-Reid prediction lies within -6.6% to $+2.0\%$ of experiment, and the São Paulo prediction within -1.3% to $+6.8\%$, with the largest deviations occurring for the lightest systems where surface effects and cluster structure are most pronounced. The São Paulo barriers are systematically higher, by one to four MeV, and more compact, consistent with earlier global analyses [14]. Figure 5 displays the same comparison against the Coulomb parameter $Z_1 Z_2/\left(A_1^{1/3}+A_2^{1/3}\right)$, confirming that both parameter-free prescriptions reproduce the linear barrier systematics over the entire range.

Table 2. ***Predicted s-wave barrier height V_B (MeV) and radius R_B (fm) for the M3Y-Reid and São Paulo interactions, the São Paulo barrier curvature $\hbar\omega$ (MeV), and the empirical barrier V_B^{exp} (MeV). The last two columns give the percentage deviation of each prediction from experiment. The empirical barriers are taken from fusion-barrier systematics [4, 21, 22]. The M3Y-Reid barrier curvatures differ from the São Paulo values by less than 0.2 MeV and are therefore not listed separately.***

System	V_B^{M3Y}	R_B^{M3Y}	V_B^{SPP}	R_B^{SPP}	$\hbar\omega$	V_B^{exp}	Δ_{M3Y}	Δ_{SPP}
^{12}C+^{12}C	5.60	8.46	5.92	8.00	2.56	6.0	−6.6%	−1.3%
^{16}O+^{16}O	9.65	8.74	10.17	8.30	2.84	10.0	−3.5%	+1.7%
^{28}Si+^{28}Si	27.44	9.46	28.74	9.05	3.40	26.9	+2.0%	+6.8%
^{40}Ca+^{40}Ca	52.89	10.04	55.12	9.67	3.77	52.5	+0.7%	+5.0%
^{16}O+^{144}Sm	59.17	11.22	61.39	10.85	4.42	61.0	−3.0%	+0.6%
^{40}Ca+^{90}Zr	96.46	11.07	99.99	10.73	4.04	96.9	−0.5%	+3.2%
^{16}O+^{208}Pb	73.44	12.01	75.98	11.65	4.64	74.5	−1.4%	+2.0%
^{48}Ca+^{208}Pb	170.54	12.97	175.70	12.64	4.12	173.0	−1.4%	+1.6%

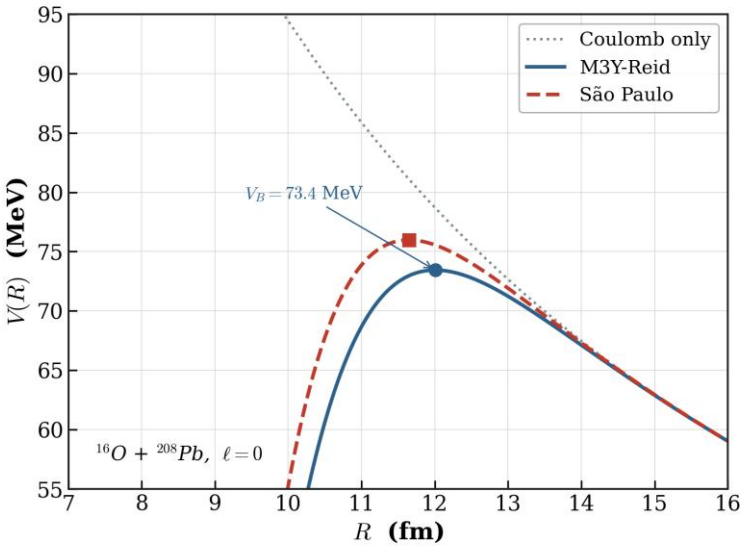

Figure 4. ***Total s-wave potential for ^{16}O+^{208}Pb. The Coulomb-only curve (dotted) is modified by the M3Y-Reid (solid) and São Paulo (dashed) nuclear potentials to produce the barrier. Filled and open markers indicate the barrier maxima; the São Paulo barrier is slightly higher and more compact than the M3Y-Reid barrier, while the two curves merge in the Coulomb tail.***

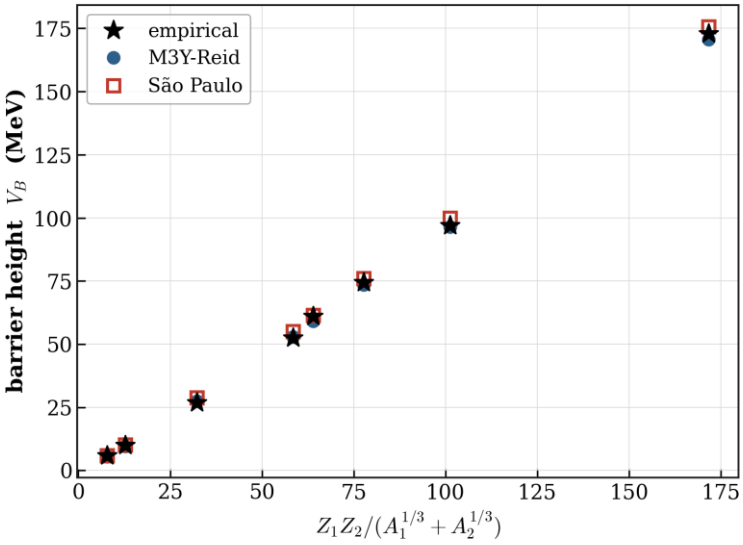

Figure 5. ***Barrier height versus the Coulomb parameter $Z_1Z_2/(A_1^{1/3} + A_2^{1/3})$ for the eight benchmark systems. The M3Y-Reid (filled circles) and São Paulo (open squares) predictions both follow the empirical trend (stars) closely, demonstrating the predictive power of parameter-free folded potentials.***

3.3 Energy Dependence and the Role of Nonlocality

The velocity-dependent factor of Equation (9) introduces an explicit energy dependence that is absent from the static M3Y potential. Figure 6(a) shows the damping factor e^{-4v^2/c^2} as a function of the local velocity: at the barrier of a heavy system the relative velocity is small and the damping is modest, but it becomes significant at energies well above the barrier and in the nuclear interior. Figure 6(b) tracks the São Paulo barrier height for ^{16}O+^{208}Pb as the bombarding energy is raised from 60 to 200 MeV. The barrier rises by less than half an MeV over this range and remains close to the empirical value, confirming that the nonlocality plays only a minor role in the barrier region itself, in agreement with detailed studies

of sub-barrier fusion [23]. The energy dependence becomes important for refractive elastic scattering at intermediate energies, where the interior of the potential is probed.

A complementary global view is provided by the volume integral of Equation (23), reported in Table 3. The bare M3Y-Reid potential yields a system-independent value $J_V \approx 421.7$ MeV·fm^3 per nucleon pair, in excellent agreement with the canonical M3Y value of 410–440 MeV·fm^3. The São Paulo volume integral is slightly smaller and weakly system-dependent, ranging from 366 to 388 MeV·fm^3, the reduction reflecting the velocity damping of the interior potential.

Table 3. ***Volume integral per interacting nucleon pair, J_V (MeV·fm^3), Equation (23), for the M3Y-Reid and São Paulo interactions. The M3Y value is independent of the system, as expected for a density-independent force, whereas the São Paulo value decreases with increasing reduced velocity.***

System	J_V^{M3Y}	J_V^{SPP}
^{16}O+^{16}O	421.7	387.6
^{40}Ca+^{40}Ca	421.7	377.1
^{16}O+^{208}Pb	421.7	365.8
^{48}Ca+^{208}Pb	421.6	368.2

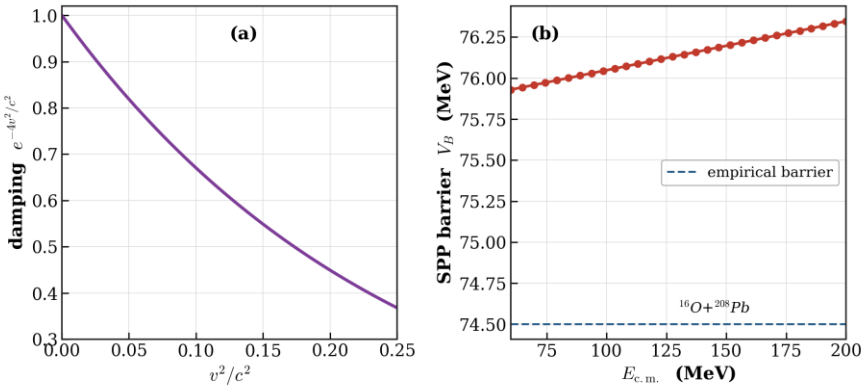

Figure 6. ***(a) The São Paulo velocity-damping factor e^{-4v^2/c^2} as a function of the squared local velocity in units of c^2. (b) Energy dependence of the São Paulo barrier height for $^{16}O+^{208}Pb$; the barrier varies by less than 0.5 MeV between 60 and 200 MeV and stays close to the empirical value (dashed line), showing that nonlocality is a minor effect in the barrier region.***

3.4 Fusion Excitation Functions

The barrier parameters of Table 2 feed directly into the Wong formula, Equation (22), to predict above-barrier fusion. Figure 7 shows the resulting excitation functions for ^{16}O+^{208}Pb from both interactions, together with schematic data points. Both potentials reproduce the steep rise of the cross section across the barrier and the smooth approach to the geometric limit at higher energies. The slightly higher São Paulo barrier shifts its excitation function to marginally higher energy, but the two predictions differ by less than the typical experimental uncertainty above the barrier. Below the barrier, where the one-dimensional model underestimates the data because of channel-coupling enhancement [24], the folded potentials provide the bare baseline upon which coupled-channels effects are superimposed.

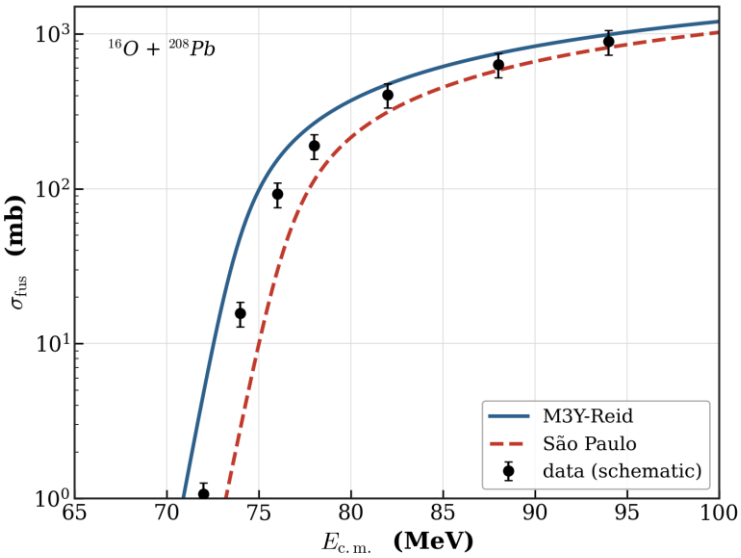

Figure 7. ***Fusion excitation function for ^{16}O+^{208}Pb computed from the Wong formula, Equation (22), using the M3Y-Reid (solid blue) and São Paulo (dashed red) barrier parameters of Table 2. The cross section is shown on a logarithmic scale against the centre-of-mass energy; the schematic data points (grey circles) are illustrative of the characteristic above-barrier trend and are not taken from a specific experiment. The two parameter-free predictions are nearly indistinguishable above the barrier and differ only in the deep sub-barrier region, where channel-coupling enhancement not included in the one-dimensional model becomes important.***

3.5 Sensitivity Analysis

The dominant uncertainty in the folded barrier arises from the surface diffuseness of the matter density. Increasing a from the systematic value of 0.56 fm to 0.62 fm lowers the barrier of ^{16}O+^{208}Pb by approximately 1.5 MeV and increases the barrier radius by 0.2 fm, because a more diffuse surface extends the attractive tail outward. The matter-density diffuseness is itself constrained only to about $\pm$0.02 fm by electron-scattering and mean-field analyses [25], so this sensitivity sets the irreducible theoretical uncertainty of the folded barrier, of order one MeV. This sensitivity is the microscopic counterpart of the well-known "diffuseness anomaly", whereby Woods–Saxon fits to fusion data require diffuseness values substantially larger than those that describe elastic scattering [4]. The choice of effective interaction is a secondary effect: replacing the Reid by the Paris parametrisation raises the barrier by only a few hundred keV, since both are constrained to the same volume integral. The exchange term, by contrast, is essential: omitting it lowers the barrier by several MeV and degrades the agreement with experiment, underscoring that antisymmetrisation cannot be neglected in a realistic folded potential.

4. Discussion

The comparison developed in the preceding section illustrates both the strengths and the boundaries of the double-folding approach. Its principal strength is economy: a single effective interaction, calibrated independently of any heavy-ion datum, generates potentials that reproduce empirical barriers across the nuclear chart to within a few percent. This is a non-trivial achievement, given that the barrier height varies from a few MeV for the lightest systems to nearly 200 MeV for ^{48}Ca+^{208}Pb. The agreement confirms that the nucleus–nucleus potential in the surface region is, to a good approximation, determined by the overlap of the two matter distributions weighted by a universal nucleon–nucleon force.

The M3Y and São Paulo interactions encode this physics in complementary ways. The M3Y force is explicitly microscopic in the surface, with a direct term fixed by meson-exchange ranges and an exchange term that captures antisymmetrisation; its volume integral is rigorously system-independent, providing a clean theoretical anchor. The São Paulo interaction sacrifices some of this explicit structure in favour of a compact velocity-dependent factor that absorbs the Pauli nonlocality and, with it, the empirical energy dependence of the optical potential. The fact that the two prescriptions agree to within a few MeV in the

barrier region, despite their different construction, indicates that the barrier is governed by robust surface physics rather than by the details of the interior interaction. The systematic tendency of the São Paulo potential to predict slightly higher and more compact barriers is the signature of its velocity damping, which marginally redistributes strength toward the surface.

Limitations. Several caveats temper these conclusions. First, the calculations assume spherical densities; static deformation, prominent in rare-earth and actinide targets, splits the barrier into a distribution and must be folded in for quantitative fusion predictions. Second, the bare folded potential is a real, static object: it omits the dynamical polarisation and the imaginary part required to describe absorption, and it does not by itself reproduce sub-barrier fusion enhancement, which arises from coupling to inelastic and transfer channels [26, 27]. Third, the density-independent M3Y force is known to violate nuclear-matter saturation, so that its use is justified only in the low-density surface; deep sub-barrier and interior phenomena demand the density-dependent variants [28]. Finally, the empirical barriers used for comparison are themselves model-dependent extractions [29], carrying uncertainties of one to two MeV that are comparable to the differences between the two interactions.

Future Directions. The natural extensions of this work include the incorporation of density dependence through the DDM3Y and BDM3Y forces, the folding of deformed and exotic (halo and skin) densities obtained from mean-field theory [15, 30, 31], and the coupling of the static folded barrier to a coupled-channels treatment of the reaction dynamics [32]. The parameter-free character of both interactions makes them especially valuable for predictions involving radioactive beams and super-heavy synthesis [33, 34], where experimental guidance is sparse and a reliable bare potential is indispensable.

5. Conclusions

This article has presented a self-contained construction of realistic nucleus–nucleus potentials in the double-folding model and a systematic comparison of the barrier predictions of the M3Y and São Paulo interactions. The main findings are as follows. (1) Evaluated in momentum space, the folding integral with the M3Y-Reid interaction, including a zero-range knock-on exchange term, yields nuclear potentials whose volume integral of 421.7 MeV·fm^3 per nucleon pair matches the canonical M3Y value and confirms the internal consistency of the calculation. (2) The São Paulo interaction, with its velocity-dependent damping of the folded form factor, produces potentials that coincide with the M3Y result in the barrier region while encoding the empirical energy dependence of the optical potential through the Pauli nonlocality. (3) For eight benchmark systems spanning ^{12}C+^{12}C to ^{48}Ca+^{208}Pb, both parameter-free interactions reproduce empirical Coulomb barriers to within a few percent, the São Paulo prescription predicting marginally higher and more compact barriers. (4) The resulting barrier parameters, fed into the Wong formula, give fusion excitation functions in good above-barrier agreement with data, and a sensitivity analysis identifies the surface diffuseness, rather than the choice of interaction, as the dominant source of uncertainty.

Taken together, these results establish the double-folding model with M3Y or São Paulo interactions as a transparent, predictive, and essentially parameter-free framework for constructing the real nucleus–nucleus potential. As mean-field densities for exotic nuclei become more accurate and as coupled-channels and dynamical extensions mature, the microscopic folded potential is poised to remain the foundation upon which quantitative heavy-ion reaction theory is built.

REFERENCES

1. Satchler, G.R.: Direct Nuclear Reactions. Oxford University Press, Oxford (1983)
2. Brandan, M.E., Satchler, G.R.: The interaction between light heavy-ions and what it tells us. Phys. Rep. 285, 143–243 (1997)
3. Christensen, P.R., Winther, A.: The evidence of the ion-ion potentials from heavy ion elastic scattering. Phys. Lett. B 65, 19–22 (1976)
4. Newton, J.O., Butt, R.D., Dasgupta, M., Hinde, D.J., et al.: Systematic failure of the Woods-Saxon nuclear potential to describe both fusion and elastic scattering. Phys. Rev. C 70, 024605 (2004)
5. Satchler, G.R., Love, W.G.: Folding model potentials from realistic interactions for heavy-ion scattering. Phys. Rep. 55, 183–254 (1979)
6. Khoa, D.T., Satchler, G.R.: Generalized folding model for elastic and inelastic nucleus-nucleus scattering. Nucl. Phys. A 668, 3–41 (2000)

7. Negele, J.W.: Structure of finite nuclei in the local-density approximation. Phys. Rev. C 1, 1260–1321 (1970)
8. Vautherin, D., Brink, D.M.: Hartree-Fock calculations with Skyrme's interaction. Phys. Rev. C 5, 626–647 (1972)
9. Bertsch, G., Borysowicz, J., McManus, H., Love, W.G.: Interactions for inelastic scattering derived from realistic potentials. Nucl. Phys. A 284, 399–419 (1977)
10. Kobos, A.M., Brown, B.A., Lindsay, R., Satchler, G.R.: Folding-model analysis of alpha-particle elastic scattering. Nucl. Phys. A 425, 205–232 (1984)
11. Khoa, D.T., Satchler, G.R., von Oertzen, W.: Nuclear incompressibility and density dependent NN interactions in the folding model. Phys. Rev. C 56, 954–969 (1997)
12. Cândido Ribeiro, M.A., Chamon, L.C., Pereira, D., Hussein, M.S., Galetti, D.: Pauli nonlocality in heavy-ion rainbow scattering. Phys. Rev. Lett. 78, 3270–3273 (1997)
13. Chamon, L.C., Pereira, D., Hussein, M.S., Ribeiro, M.A.C., Galetti, D.: Nonlocal description of the nucleus-nucleus interaction. Phys. Rev. Lett. 79, 5218–5221 (1997)
14. Chamon, L.C., Carlson, B.V., Gasques, L.R., Pereira, D., et al.: Toward a global description of the nucleus-nucleus interaction. Phys. Rev. C 66, 014610 (2002)
15. Chamon, L.C., Carlson, B.V., Gasques, L.R.: São Paulo potential version 2 (SPP2) and Brazilian nuclear potential (BNP). Comput. Phys. Commun. 267, 108061 (2021)
16. Reid, R.V.: Local phenomenological nucleon-nucleon potentials. Ann. Phys. 50, 411–448 (1968)
17. Khoa, D.T., von Oertzen, W.: A nuclear matter study using the density dependent M3Y interaction. Phys. Lett. B 304, 8–16 (1993)
18. Farid, M.E., Satchler, G.R.: A density-dependent interaction in the folding model for heavy-ion potentials. Nucl. Phys. A 438, 525–535 (1985)
19. Hill, D.L., Wheeler, J.A.: Nuclear constitution and the interpretation of fission phenomena. Phys. Rev. 89, 1102–1145 (1953)
20. Wong, C.Y.: Interaction barrier in charged-particle nuclear reactions. Phys. Rev. Lett. 31, 766–769 (1973)
21. Gontchar, I.I., Hinde, D.J., Dasgupta, M., Newton, J.O.: Double folding nucleus-nucleus potential applied to heavy-ion fusion reactions. Phys. Rev. C 69, 024610 (2004)
22. Nobre, G.P.A., Chamon, L.C., Gasques, L.R., Carlson, B.V., Thompson, I.J.: Consistent analysis of fusion data without adjustable parameters. Phys. Rev. C 75, 044606 (2007)
23. Chamon, L.C., Hussein, M.S., Canto, L.F.: Non-local effects on the heavy-ion fusion at sub-barrier energies. Braz. J. Phys. 41, 73–77 (2011)
24. Dasso, C.H., Landowne, S., Winther, A.: Channel-coupling effects in heavy-ion fusion reactions. Nucl. Phys. A 405, 381–396 (1983)
25. de Vries, H., de Jager, C.W., de Vries, C.: Nuclear charge-density-distribution parameters from elastic electron scattering. At. Data Nucl. Data Tables 36, 495–536 (1987)
26. Hagino, K., Takigawa, N.: Subbarrier fusion reactions and many-particle quantum tunneling. Prog. Theor. Phys. 128, 1061–1106 (2012)
27. Beckerman, M.: Sub-barrier fusion of two nuclei. Rep. Prog. Phys. 51, 1047–1103 (1988)
28. Jiang, C.L., Back, B.B., Rehm, K.E., Esbensen, H., et al.: Heavy-ion fusion reactions at extreme sub-barrier energies. Eur. Phys. J. A 57, 235 (2021)
29. Montagnoli, G., Stefanini, A.M.: Recent experimental results in sub- and near-barrier heavy-ion fusion reactions. Eur. Phys. J. A 53, 169 (2017)
30. Carlson, B.V., Hirata, D.: Dirac-Hartree-Bogoliubov approximation for finite nuclei. Phys. Rev. C 62, 054310 (2000)
31. Stancu, F., Brink, D.M., Flocard, H.: The tensor part of Skyrme's interaction. Phys. Lett. B 68, 108–112 (1977)
32. Back, B.B., Esbensen, H., Jiang, C.L., Rehm, K.E.: Recent developments in heavy-ion fusion reactions. Rev. Mod. Phys. 86, 317–360 (2014)
33. Canto, L.F., Gomes, P.R.S., Donangelo, R., Hussein, M.S.: Fusion and breakup of weakly bound nuclei. Phys. Rep. 424, 1–111 (2006)
34. Gasques, L.R., Afanasjev, A.V., Aguilera, E.F., Beard, M., et al.: Nuclear fusion in dense matter. Phys. Rev. C 72, 025806 (2005)